Journal of Peptide Science
J. Pept. Sci. (2007)
Published online in Wiley InterScience (www.interscience.wiley.com). DOI: 10.1002/psc.968

JOURNAL OF PEPTIDE SCIENCE

Live-cell analysis of cell penetration ability and toxicity of oligo-arginines‡

GISELA TÜNNEMANN,[a] GOHAR TER-AVETISYAN,[a] ROBERT M. MARTIN,[a] MARTIN STÖCKL,[b] ANDREAS HERRMANN[b] and M. CRISTINA CARDOSO[a]*

[a] Max Delbrueck Center for Molecular Medicine, D-13125 Berlin, Germany
[b] Institute of Biology/Biophysics, Humboldt University of Berlin, D-10115 Berlin, Germany

Received 9 July 2007; Revised 21 September 2007; Accepted 1 October 2007

Abstract: Cell penetrating peptides (CPPs) are useful tools to deliver low-molecular-weight cargoes into cells; however, their mode of uptake is still controversial. The most efficient CPPs belong to the group of arginine-rich peptides, but a systematic assessment of their potential toxicity is lacking. In this study we combined data on the membrane translocation abilities of oligo-arginines in living cells as a function of their chain length, concentration, stability and toxicity. Using confocal microscopy analysis of living cells we evaluated the transduction frequency of the L-isoforms of oligo-arginines and lysines and then monitored their associated toxicity by concomitant addition of propidium iodide. Whereas lysines showed virtually no transduction, the transduction ability of arginines increased with the number of consecutive residues and the peptide concentration, with L-R9 and L-R10 performing overall best. We further compared the L- and D-R9 isomers and found that the D-isoform always showed a higher transduction as compared to the L-counterpart in all cell types. Notably, the transduction difference between D- and L-forms was highly variable between cell types, emphasizing the need for protease-resistant peptides as vectors for drug delivery. Real-time kinetic analysis of the D- and L-isomers applied simultaneously to the cells revealed a much faster transduction for the D-variant. The latter underlies the fact that the isomers do not mix, and penetration of one peptide does not perturb the membrane in a way that gives access to the other peptide. Finally, we performed short- and long-term cell viability and cell cycle progression analyses with the protease-resistant D-R9. Altogether, our results identified concentration windows with low toxicity and high transduction efficiency, resulting in fully bioavailable intracellular peptides. Copyright © 2007 European Peptide Society and John Wiley & Sons, Ltd.

Supplementary electronic material for this paper is available in Wiley InterScience at http://www.interscience.wiley.com/jpages/1075-2617/suppmat/

Keywords: arginine-rich peptides; cell cycle; cell penetrating peptides; cell viability; membrane integrity; membrane translocation; oligo-lysines; oligo-arginines

INTRODUCTION

Cell penetrating peptides (CPPs) possess the unique ability to shuttle linked cargoes such as drugs [1], peptides [2–6], proteins [7–9], peptide nucleic acids (PNAs) [10–12] and nanoparticles [13,14] across the plasma membrane which is otherwise virtually impermeable for hydrophilic compounds. CPPs can be subdivided into two major groups: model amphiphilic peptides (MAPs) [15,16] developed on the basis of spatial separation of positively charged and hydrophobic amino acid residues; and arginine-rich peptides (R-RPs) delineated from natively occurring minimal transduction domains of proteins, e.g. TAT from HIV-1 TAT protein [7,17–19] and penetratin from the homeobox of antennapedia protein [20–22]. However, plasma membrane translocation of MAPs structurally requires at least four helical turns but does not depend on the positively charged amino acid residues [15], whereas the transduction ability of R-RPs depends on a minimum number of arginines [23,24], suggesting that the entry mechanisms of both types of CPPs are unrelated. The translocation ability of R-RPs does not seem to be solely a matter of charge, but has been proposed to reside in the guanidinium group of the arginine itself [25]. The formation of lipophilic ion pairs with abundant sulfate, phosphate or carboxylate groups of membrane constituents via the two amino functions of arginine provides a mechanistic framework for the translocation of a highly charged compound through the plasma membrane [26]. CPP-mediated delivery of cargoes into the cytoplasm can be achieved by at least two independent mechanisms: (i) adsorptive endocytosis and subsequent release of the enclosed compounds from endosomes or lysosomes [7,27–29]; and (ii) rapid crossing of the membrane by a seemingly energy-independent, not-well-understood mechanism referred to as transduction [5,30–32]. Whereas R-RPs coupled

* Correspondence to: M. Cristina Cardoso, Max Delbrueck Center for Molecular Medicine, Robert-Roessle-Str. 10, D-13125 Berlin, Germany; e-mail: cardoso@mdc-berlin.de
‡ This article is part of the Special Issue of the Journal of Peptide Science entitled "2nd workshop on biophysics of membrane-active peptides".

to high-molecular-weight cargoes are restricted to the endocytic mode of uptake [5,33,34], R-RPs themselves or interconnected to low-molecular-weight cargoes have both options. Above a certain concentration (transduction threshold), which varies between 1 and 10 M depending on the cell type and the size of the cargo [5], R-RPs directly translocate across the plasma membrane into the cell. Several live-cell studies have shown that functional peptides attached to R-RPs exert biological effects after the transduction event [2–6]. Importantly, R-RP-mediated transduction circumvents the inefficient step of release from cytoplasmic vesicles after the endocytic uptake. However, a systematic evaluation of the cell penetration ability, in combination with an assessment of potential short- and long-term toxic effects of R-RPs, is lacking. In this study, we combined data on the membrane translocation abilities of oligo-arginines in living cells as a function of their chain length, concentration, stability and toxicity.

MATERIAL AND METHODS

Peptides

Consecutive arginines (5–12) and lysines (5–12) as L-isomers and TAMRA-R9 and Fluos-R10 also as D-isomers were synthesized and coupled directly to fluorescein (Fluos) or 5,6-TAMRA at the *N*-terminus by Peptide Specialty Laboratories GmbH (Heidelberg, Germany). The peptides were purified by HPLC and their appropriate masses confirmed by mass spectrometry. The isoelectric points (p*I*) were estimated using the freeware tool ProtParam.

Cells

All cell types were cultured in Dulbecco's modified Eagle medium (DMEM) with fetal calf serum (FCS) (Life Technologies, Inc., USA) at the following concentrations: C2C12 mouse myoblasts 20%, human HeLa cells 10%, MDCKII dog epithelial kidney cells 10% and BJ-hTERT human fibroblasts 10%. Primary cultures from male WKY rats aged 3 months were performed as described previously [35].

Transduction Experiments

As peptide transduction is influenced by the peptide-to-cell ratio [36], for all transduction experiments μ-Slide VI observation chambers were used (Ibidi, Martinsried, Germany), which guarantee a defined and equal liquid volume above the cells throughout the entire observation channel. The respective cell types were seeded at 70% confluency into the observation chambers and incubated overnight at 37 C at 5% CO_2. Special care was taken that cell densities were equal throughout sets of experiments. The oligo-arginines and oligo-lysines were diluted in DMEM medium without FCS to avoid precipitation of the peptides. For the chain-length-dependent transduction assay, 2 g/ml propidium iodide (PI) was added directly to the diluted peptide solution prior to the transduction experiment. The culture medium was gently aspirated from the cells and exchanged against the respective peptide dilutions in a volume of 60 l. The cells were kept for 1 h in the incubator until imaging at the microscope under the same conditions. For each peptide concentration, between 140 and 250 cells were analyzed and the experiments were performed in duplicate. The images were collected with two different laser settings, one set resulting in images without overexposed signals and one set with higher laser intensities, so that weaker signals could not be missed. The microscope settings per concentration and within these two sets were identical. Acquired images were analyzed visually, and cells unambiguously showing fluorescent signal inside the nucleus were scored as transduced. The graphics were generated using the Origin version 7.5 software (OriginLab Corp., Northampton, USA).

Cell Cycle and Viability Assays

For the modified (3-(4,5-dimethylthiazol-2-yl)-2,5 diphenyl-tetrazolium-bromide (MTT) assay, C2C12 cells were incubated for 2 h with different concentrations of the peptides D-R9 and L-R9. MTT was dissolved at 0.4 mg/ml in DMEM. Subsequently, the cells were washed once, followed by addition of 100 l of the MTT solution and were returned to the incubator for 5 h. Cells were then analyzed by confocal laser scanning microscopy (CLSM). The transduction frequency was monitored by the fluorescence of the Fluos- or TAMRA-labeled peptides, respectively, and the formation of the blue-violet formazan complex was monitored by excitation with 488 nm and detection in the transmission channel. For each peptide concentration, five fields of view with a 40× objective corresponding to a total number of ~150 cells were collected. Cells with less formazan signal intensity than the control cells were counted as nonviable.

For the analysis of the plasma membrane integrity during and after transduction, we used 2 g/ml PI mixed together with the transducing peptides in DMEM to detect transient pore formation or membrane perturbations, and 0.5% (V/V) trypan blue to distinguish, after the transduction period of 2 h, the cells with permanently compromised membranes. Data were displayed by using Microsoft Excel.

To analyze relatively short-term effects on DNA condensation by the peptides, C2C12 cells were preincubated for 10 min with the DNA dye DRAQ5 (Biostatus Limited, UK) as described [37] and then incubated with different concentrations of the D-R9 peptide. Cells were imaged by CLSM before and after the treatment. Long-term effects on the cell cycle progression were determined by fluorescence activated cell sorting (FACS) analysis of PI-stained C2C12 cells. For this purpose, C2C12 cells were plated onto 150 mm diameter dishes and incubated with different concentrations of the respective peptides at a density of 40% in DMEM for 2 h. Then the medium was replaced by DMEM with 20% FCS and the cells were cultivated for further 16 h until they reached a density of 60%. For FACS analysis the cells were trypsinized, washed with PBS, fixed with ice-cold 90% EtOH, washed with PBS, treated with 0.1 mg/ml RNAse and stained with 33 g/ml PI, and DNA content was measured with a FACSCalibur (Becton Dickinson). Data were analyzed and plotted with the flow cytometry software FLOWJO (Tree Star, Inc., USA).

DOI: 10.1002/psc

Microscopy, Image Acquisition and Analysis

Confocal images were acquired with a Zeiss confocal laser scanning microscope, LSM510 Meta, mounted on an Axiovert 200M inverted microscope equipped with a live-cell microscope incubation cage (Okolab, Italy) using either a 40× plan-neofluar NA1.3 or a 63× plan-apochromat NA1.4 oil-immersion, phase-contrast objectives. For all settings the main beam splitter was HFT UV/488/543/633, and the specific parameters for the single fluorophores were as follows: Fluos, excited at 488 nm, detected with a 500–530 nm band-pass filter; TAMRA, excited at 543 nm, detected with 565–615 nm band-pass filter; and trypan blue, PI and DRAQ5, excited with 633 nm, detected with 650 nm long-pass filter. Phase contrast images were recorded with excitation at 488 nm and detection in the transmission channel. Laser power for observation was typically 1–5% (488 nm, 25 mW), 50–60% (543 nm, 1 mW) and 3–5% (633 nm, 5 mW) unless otherwise indicated. Settings were adjusted in a way that image pixels were not over- or underexposed with the range indicator function in the Zeiss LSM software version 3.2. To ensure that weak intracellular fluorescence signals of the peptides were not missed, a set of overexposed images were collected in addition.

RESULTS AND DISCUSSION

The decisive role of arginine clusters for translocation over the plasma membrane has been known for some time. Therefore, several studies were aimed at determining the optimal number of arginines or minimal structural requirements that permit efficient transduction. Surprisingly, most of them analyzed either fixed cells [23,24,38] and/or used FACS analysis without a protocol to efficiently remove the cationic peptides sticking to the extracellular side of the plasma membrane [39]. To exclude the above artifacts, we analyzed the transduction frequency of oligo-arginines and -lysines with chain length from 5 to 12 directly by CLSM of living cells. In addition, we compared only data from experiments using the same incubation times for all peptides and at the same cell density and varied only the concentrations for each peptide. Figure 1(A) displays the possible uptake phenotypes of C2C12 mouse myoblasts after addition of the fluorescent peptide for 1 h. The images on the left side, upper panel, show cells that endocytosed the L-R9 peptide incubated at a concentration of 10 M, where the fluorescence of the peptide solely resided in cytoplasmic vesicles, and no free cytoplasmic peptide was detectable by means of fluorescence microscopy. The images on the right side, upper panel, depict cells that incorporated L-R6 peptide added at a concentration of 50 M with fluorescence detected throughout the cytoplasm and nucleus, which we hereafter refer to as transduction. Cells with mixed phenotypes (Figure 1(A), lower panel) that show in addition to transduction vesicular uptake were also scored as transduced cells. Only the uptake mode of transduction yields peptide available in all intracellular compartments and, therefore, is able to reach all potential targets. In order to detect any possible membrane perturbations or transient pore formation, the vital dye PI was added to mouse myoblast cultures simultaneously with the oligo-arginines (see scheme in Figure 1(A)). The plots in Figure 1(B) summarize the transduction results for all oligo-arginine peptides. None of the oligo-arginines tested (R5–R12) was able to transduce at a concentration of 0.5, 1 or 5 M in a total volume of 60 l. Transduction could be observed at 10 M for the peptides R8–R12, with frequencies over 50% for the peptides R10–R12. Whereas R5 did not transduce over the whole concentration range tested (between 0.5 to 100 M), R6 appeared intracellularly only in 4% of the cells at 50 M and 28% at 100 M. R7–R9 transduced between 18 and 42% of the cells at 50 M and reached frequencies between 75 and 90% at 100 M. The peptides R10–R12 transduced already to a level of 70–90% at 10 M concentration and the percentage of transduction increased only slightly at 5- or 10-fold higher concentration. In stark contrast, either no or very low frequency of cell penetration could be detected with all the oligo-lysines tested (K5–K12) at an even wider concentration range (data not shown). The uptake of PI by the oligo-arginine transduced cells (Figure 1(B)) indicated severe toxicity only with R8, R10, R11 and R12 at the highest peptide concentration tested (100 M) and for R11 and R12 already at 50 M. For the transducing peptides with lower chain length, the percentage of PI-stained cells in all cases was below 10%. At 10 M, except for R12 all transducing peptides caused no membrane damage that could be detected by simultaneous PI staining. Notably, PI was not observed inside transduced cells by peptides with a low number of arginines or at low concentrations. This fact argues against the formation of transient pores or strong membrane perturbations. Whereas previous studies found an optimum number of consecutive arginines for transduction [24,38], our results support a linear dependence of the transduction frequencies on the number of consecutive arginines. Considering also the PI uptake data, R9 or R10 peptides combine a medium to high transduction level associated with a tolerable toxicity. To verify and extend our live-cell analysis, we selected three oligo-arginine peptides (namely, R5, R7 and R9) and tested their uptake potential into artificial membranes. The R5 peptide was chosen, as it did not transduce into cells, whereas the R7 was able to transduce, albeit at a low level, and R9 was the most efficient while still retaining low toxicity. The 7-nitro-2-1,3-benzoxadiazol-4-yl (NBD) labeled peptides were applied to large unilamellar vesicles (LUVs) and the percentage of transduced peptide over time was measured with a spectrofluorometer after quenching the outer fluorescence with the NBD quencher, dithionite. The percentage of transduction rose with the number of consecutive arginines in a manner

DOI: 10.1002/psc

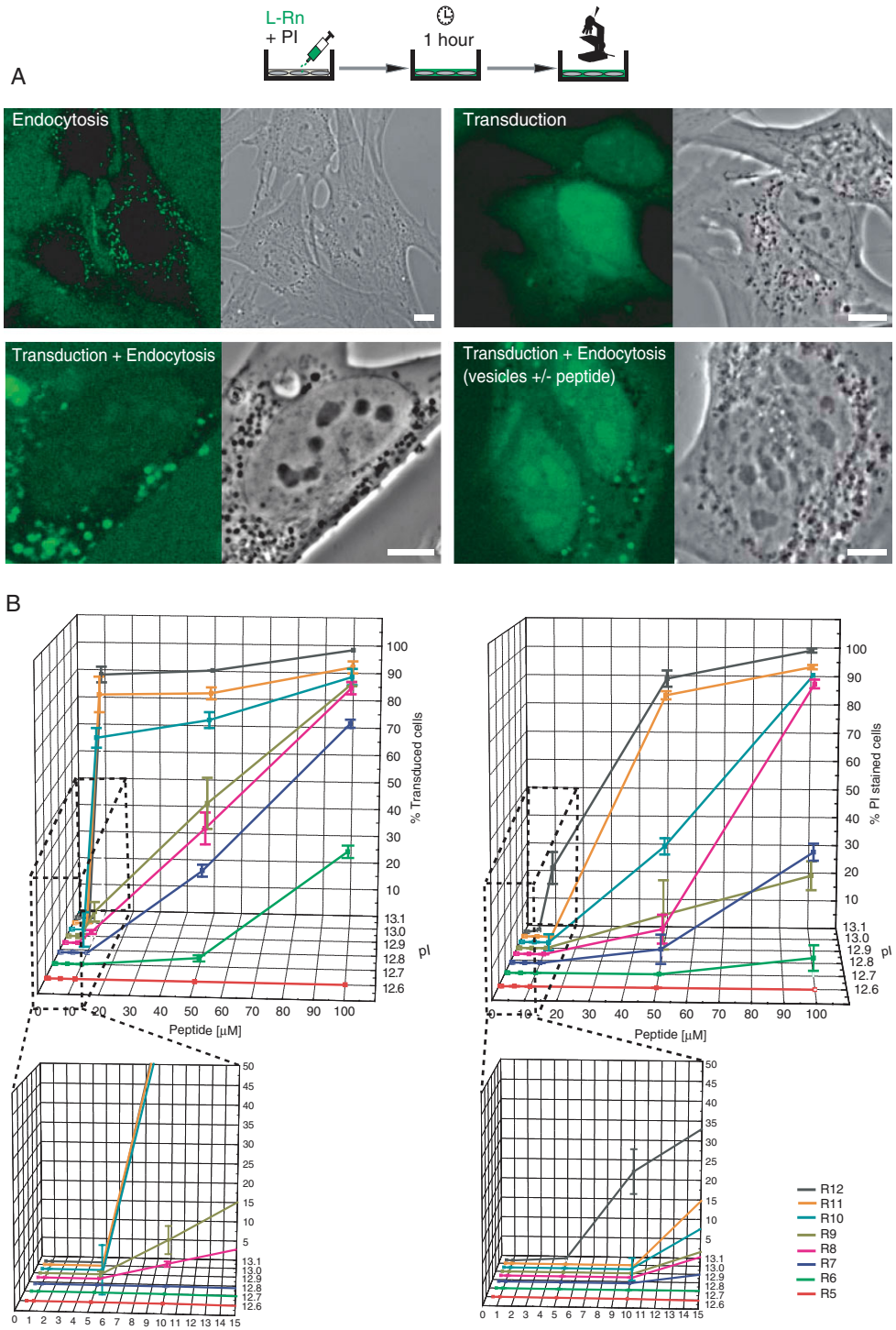

Figure 1 Assessment of dose-dependent transduction frequency of oligo-arginine peptides. (A) Confocal microscopy images displaying examples of endocytic uptake (upper, left panel, L-R9 at 10 M) *versus* transduction (upper, right panel, L-R6 at 50 M) of oligo-arginines (L-R*n*; $n = 5–12$) into mouse C2C12 myoblasts. Two mixed forms of transduction + endocytosis are shown below: transduction and endocytic peptide vesicles (left panel L-R9 at 10 M) *versus* transduction and peptide enclosed in endocytic vesicles (+) as well as excluded from endocytic vesicles (–) (right panel L-R6 at 50 M). Scale bars 10 m. The experimental procedure is shown above. Only cells showing the transduction mode of uptake (including the mixed phenotypes shown in the lower panels) were counted for the quantification in B. (B) The peptide transduction frequency shown as a fraction of C2C12 cells (in %) was scored as explained in A. Peptide transduction frequencies are shown plotted against peptide concentration (0.5, 1, 5, 10, 50, 100 M) and corresponding estimated isoelectric point (p*I*). The fraction of PI-stained C2C12 cells (in %) within the transduced cell population is plotted similarly. The lower peptide concentration plots are also shown magnified for better visualization. Error bars display the standard deviation of two independent experiments. The total number of cells counted was between 140 and 250 for each experiment.

DOI: 10.1002/psc

analogous to that in the living-cell uptake analyses (Supplementary Figure S1).

Octa-, nona- and deca-arginines have been shown to transduce successfully into living cells under noninvasive conditions and at lower concentrations [31,32,40], but different cell types as well as D- and L-isomers were used in those studies. Therefore, we next assessed the influence of D- and L-isomeric forms on the transduction efficiencies in different cell types. For that purpose, we incubated different cell types of various mammalian species and also primary cells with 10 M of the TAMRA-labeled D-isomer and the Fluos-labeled L-isomer of R9 and determined the percentage of transduced cells after 1 h incubation (Figure 2(A)). In general, the transduction frequencies for the L-form in all cell types were lower than that of the D-form, illustrating that peptide stability is an important issue for transduction. By calculating the index for the percentage of cells transduced by the L-isomer divided by the percentage of cells transduced by the D-isomer, we found characteristic values for individual cell types, which most probably reflect their extracellular proteolytic activity [41]. Whereas diploid human fibroblasts were very inefficiently transduced, rat cardiomyocytes and mouse myoblasts showed higher levels of transduction for the L-form, approaching the level of the D-form. As the D-isomer of R9 reached transduction efficiencies of over 95% in all cell types, the isomer-specific differences cannot be due to cell-type-specific membrane composition. The loss of only one arginine from L-R9 would already reduce the transduction efficiency to half at a concentration of 10 M and lead to the disappearance of the transduction potential with further proteolysis (see plot in Figure 1(B)). To ensure that the different indices were not a result of the distinct fluorescent labels attached to the peptides, the same set of experiments was performed with Fluos-labeled D- and L-isomers of R10 with the same outcome (data not shown). The overview images of the different cell types after transduction also revealed that the fluorescence intensity varied between individual cells. This variation was not correlated to

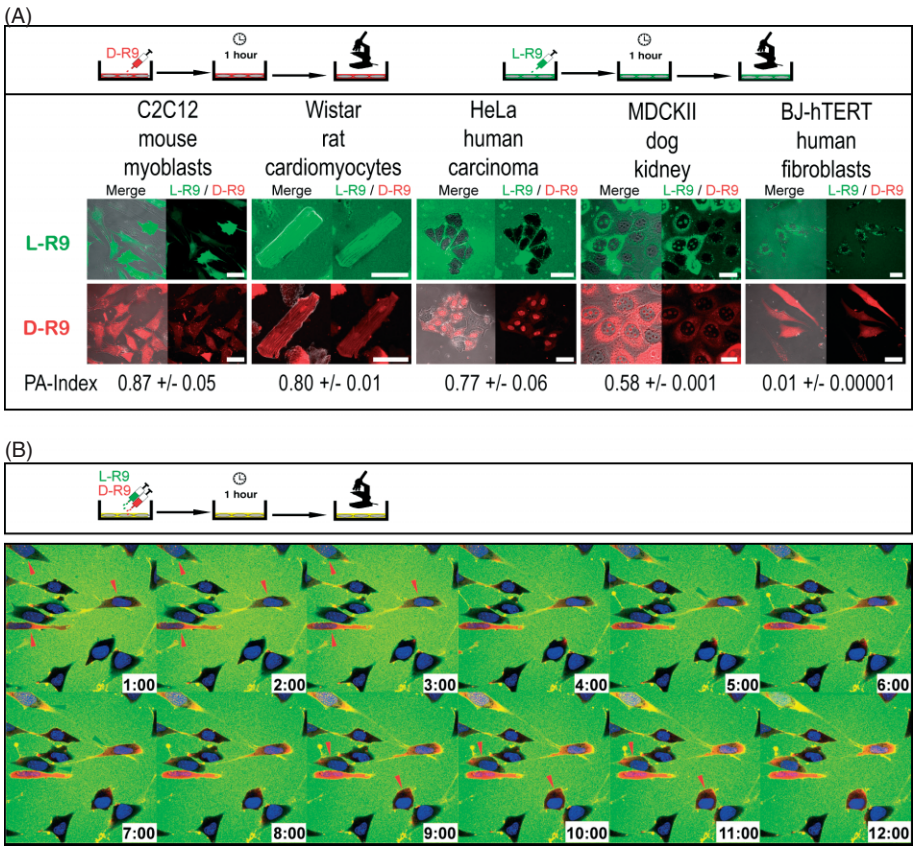

Figure 2 Cell-type-specific differences in transduction frequencies and kinetics of L- and D-isomers of R9. (A) Confocal microscopy sections of different cell types from various mammalian species 1 h after application of 10 M of the Fluos-labeled L-isomer (upper panel, green fluorescence) and the TAMRA-labeled D-isomer (lower panel, red fluorescence) of R9. For each cell type, merge images of phase contrast and fluorescence and fluorescence images alone are displayed. The index corresponds to the ratio (% transduced cells by L-isomer/% transduced cells by D-isomer) ± standard deviation. (B) Confocal microscopy time lapse (minutes : seconds) of the transduction of the L- and D-isomers of R9 simultaneously applied to C2C12 mouse myoblasts at a concentration of 10 M each. Red and green arrowheads indicate the initial detection of the transduced corresponding peptides in intracellular compartments. The cells are counterstained with the live-cell DNA dye DRAQ5 (blue). Scale bar 50 m.

DOI: 10.1002/psc

the size and, therefore, to the total accessible membrane surface of the transduced cells. Next, we tested whether kinetic differences between the transduction of D- and L-isomers occurred. For this, we applied 20 M of a 1 : 1 mixture onto mouse myoblasts and monitored the uptake in real time by CLSM. Surprisingly, several cells selectively took up the TAMRA-labeled D-isomer but not the Fluos-labeled L-form, although some cells also showed yellow color seen in the overlay of the two fluorescence images (Figure 2(B) and Movie 1). Nevertheless, the kinetics of transduction was quite different for both isomers, even though after a certain time both species had been internalized. This result argues against the formation of mixed D- and L-isomers into multimeric assemblies. We can, however, not rule out the existence of single-species multimers. In addition, no change in the transduction efficiency of the individual D- or the L- chiral forms was observed, which would be expected from the higher total peptide concentration. Finally, these data clearly show the absence of membrane damage by the penetration of one peptide species since the other species in the same cell at the same time was not taken up concomitantly.

In view of the therapeutic potential of peptide vectors for the delivery of low-molecular-weight compounds and considering the relatively high transduction rate and low percentage of PI-stained cells (Figure 1(B) and 2), we selected the nondegradable D-isomer of R9 for further detailed analysis of toxicity on mouse myoblasts. Transduction was observed starting from a concentration threshold of 5 M with a transduction frequency of about 10% (Figure 3(A)). Ten micromolar D-R9 was transduced into more than 50%, and 25 M into 70% of the cells. For concentrations of 50 and 100 M, transduction was nearly complete. Next, we examined the viability of mouse myoblasts after 2 h of incubation with different concentrations with D-R9. The ability of the cells to exclude the vital dye trypan blue was used to judge membrane integrity. Furthermore, we assessed by an MTT assay whether the transduction of D-R9 influences enzymatic activities inside the cells detected here by their ability to produce formazan [42]. Starting from the transduction threshold of 5 M, a constant decrease in viability by both assays was observed, which was mild between 5 and 25 M peptide concentration. At a concentration of 50 M, about 17% of the cells stained positive for trypan blue, and 15% of the cells produced formazan to a lesser extent than the controls. Cell death in 60% of cells resulted from 100 M of D-R9, and also the formazan levels of those cells were greatly reduced in comparison to the control cells. The slope of the trypan blue exclusion curve is steeper than that of the viability assayed by the MTT test, indicating that the membranes are the first location where massive damage occurs. Arginine-rich clusters can be found in RNA-binding proteins and are targeted to the nuclear compartment. To test long-term

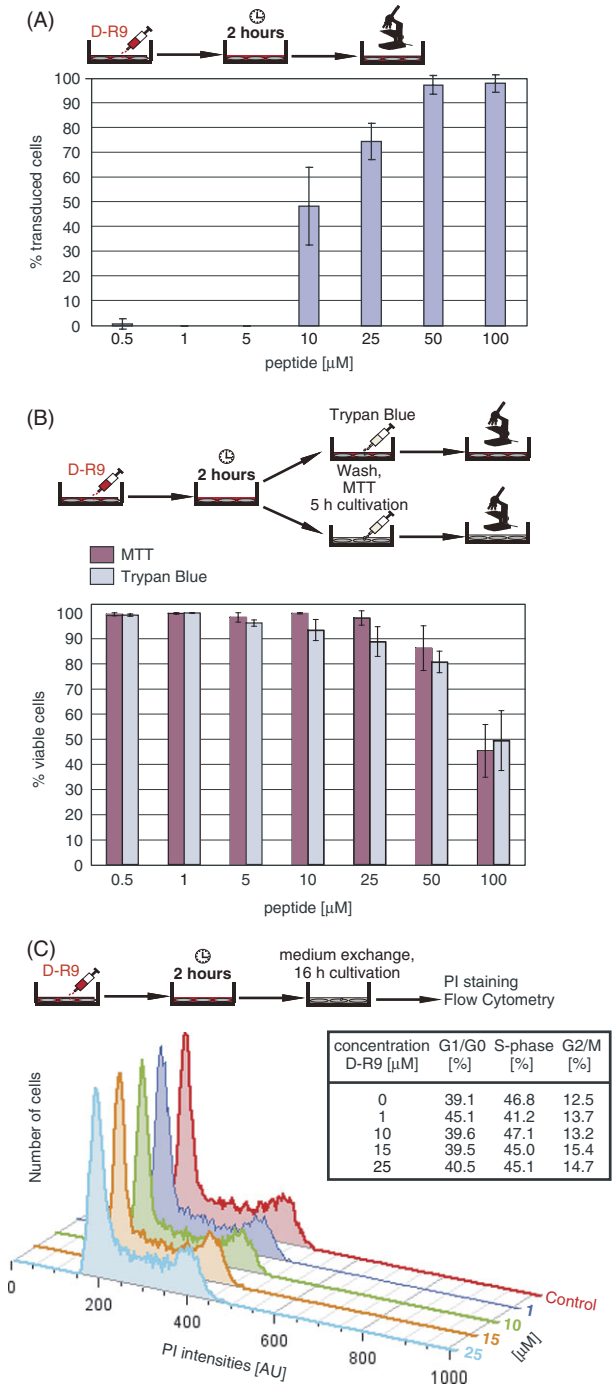

concentration D-R9 [µM]	G1/G0 [%]	S-phase [%]	G2/M [%]
0	39.1	46.8	12.5
1	45.1	41.2	13.7
10	39.6	47.1	13.2
15	39.5	45.0	15.4
25	40.5	45.1	14.7

Figure 3 Short- and long-term dose-dependent effects of D-R9 transduction on cell viability and proliferation. (A) Transduction frequencies of D-R9 in C2C12 mouse myoblasts determined as in Figure 1. (B) Cell viability determined by trypan blue exclusion and enzymatic activity MTT assay after 2 h of incubation with different concentrations of D-R9. (C) Long-term effects on the cell cycle distribution assayed by flow cytometry analysis of DNA content stained with PI. The respective experiments are explained in the schemes. For (A) and (B) the error bars display the standard deviation of two independent experiments. The total number of cells counted was between 140 and 250 for each experiment. In (C), one example of three independent experiments is depicted.

DOI: 10.1002/psc

effects on DNA replication and cell cycle progression, mouse myoblasts were incubated for 2 h with the D-R9 peptide, the medium was exchanged and they were kept in culture until the next day. Cultures were then fixed, DNA was stained with PI and the cell cycle distribution was analyzed by flow cytometry. The cell cycle profiles and the statistics are displayed in Figure 3(C) and show no concentration-dependent effect of the D-R9 peptide on the cell cycle. Altogether, the toxicological effects of the D-R9 peptide in a range of 5–25 M can be classified as mild and cell proliferation was also not affected.

CONCLUSIONS

In summary, we evaluated the transduction frequency of the L-isoforms of oligo-arginines and monitored their associated toxicity. This risk-benefit analysis of transduction led us to the selection of R9 for further analysis. With its nondegradable counterpart D-R9, we established an assay that allows the quantification of the proteolytic activity of different cell types, and emphasize the need for protease-resistant peptides as vectors for drug delivery. Importantly, the D-isoform always showed a higher transduction as compared to the L-counterpart in all cell types. The transduction difference between D- and L-forms was highly variable between cell types. Finally, our toxicity results indicate concentration windows with low toxicity and high transduction efficiency, not requiring further treatments to force endocytic vesicle rupture.

Supplementary Material

Supplementary electronic material for this paper is available in Wiley InterScience at: http://www.interscience.wiley.com/jpages/1075-2617/suppmat/

Acknowledgements

We thank I. Kocman for help with the flow cytometry, P. Domaing for excellent technical assistance and F. Witzel for her participation at the earlier stages of this project. G.T. was supported in part by the European Union (ESF Program). This work was funded by grants of the Deutsche Forschungsgemeinschaft and the Volkswagen Foundation to M.C.C.

REFERENCES

1. Nori A, Jensen KD, Tijerina M, Kopeckova P, Kopecek J. Tat-conjugated synthetic macromolecules facilitate cytoplasmic drug delivery to human ovarian carcinoma cells. *Bioconjugate Chem.* 2003; **14**: 44–50.
2. Chen CH, Gray MO, Mochly-Rosen D. Cardioprotection from ischemia by a brief exposure to physiological levels of ethanol: role of epsilon protein kinase C. *Proc. Natl. Acad. Sci. U.S.A.* 1999; **96**: 12784–12789.
3. Choi M, Rolle S, Wellner M, Cardoso MC, Scheidereit C, Luft FC, Kettritz R. Inhibition of NF-kappaB by a TAT-NEMO-binding domain peptide accelerates constitutive apoptosis and abrogates LPS-delayed neutrophil apoptosis. *Blood* 2003; **102**: 2259–2267.
4. Rohrbach S, Muller-Werdan U, Werdan K, Koch S, Gellerich NF, Holtz J. Apoptosis-modulating interaction of the neuregulin/erbB pathway with anthracyclines in regulating Bcl-xS and Bcl-xL in cardiomyocytes. *J. Mol. Cell. Cardiol.* 2005; **38**: 485–493.
5. Tünnemann G, Martin RM, Haupt S, Patsch C, Edenhofer F, Cardoso MC. Cargo-dependent mode of uptake and bioavailability of TAT-containing proteins and peptides in living cells. *FASEB J.* 2006; **20**: 1775–1784.
6. Tünnemann G, Karczewski P, Haase H, Cardoso MC, Morano I. Modulation of muscle contraction by a cell permeable peptide. *J. Mol. Med.* (in press). DOI: 10.1007/s00109-007-0238-6.
7. Fawell S, Seery J, Daikh Y, Moore C, Chen LL, Pepinsky B, Barsoum J. Tat-mediated delivery of heterologous proteins into cells. *Proc. Natl. Acad. Sci. U.S.A.* 1994; **91**: 664–668.
8. Nagahara H, Vocero-Akbani AM, Snyder EL, Ho A, Latham DG, Lissy NA, Becker-Hapak M, Ezhevsky SA, Dowdy SF. Transduction of full-length TAT fusion proteins into mammalian cells: TAT-p27Kip1 induces cell migration. *Nat. Med.* 1998; **4**: 1449–1452.
9. Schwarze SR, Ho A, Vocero-Akbani A, Dowdy SF. *In vivo* protein transduction: delivery of a biologically active protein into the mouse. *Science* 1999; **285**: 1569–1572.
10. Oehlke J, Wallukat G, Wolf Y, Ehrlich A, Wiesner B, Berger H, Bienert M. Enhancement of intracellular concentration and biological activity of PNA after conjugation with a cell-penetrating synthetic model peptide. *Eur. J. Biochem.* 2004; **271**: 3043–3049.
11. Turner JJ, Ivanova GD, Verbeure B, Williams D, Arzumanov AA, Abes S, Lebleu B, Gait MJ. Cell-penetrating peptide conjugates of peptide nucleic acids (PNA) as inhibitors of HIV-1 Tat-dependent trans-activation in cells. *Nucleic Acids Res.* 2005; **33**: 6837–6849.
12. Wolf Y, Pritz S, Abes S, Bienert M, Lebleu B, Oehlke J. Structural requirements for cellular uptake and antisense activity of peptide nucleic acids conjugated with various peptides. *Biochemistry* 2006; **45**: 14944–14954.
13. Santra S, Yang H, Stanley JT, Holloway PH, Moudgil BM, Walter G, Mericle RA. Rapid and effective labeling of brain tissue using TAT-conjugated CdS:Mn/ZnS quantum dots. *Chem. Commun.* 2005; **25**: 3144–3146.
14. Lewin M, Carlesso N, Tung CH, Tang XW, Cory D, Scadden DT, Weissleder R. Tat peptide-derivatized magnetic nanoparticles allow in vivo tracking and recovery of progenitor cells. *Nat. Biotechnol.* 2000; **18**: 410–414.
15. Scheller A, Oehlke J, Wiesner B, Dathe M, Krause E, Beyermann M, Melzig M, Bienert M. Structural requirements for cellular uptake of alpha-helical amphipathic peptides. *J. Pept. Sci.* 1999; **5**: 185–194.
16. Oehlke J, Scheller A, Wiesner B, Krause E, Beyermann M, Klauschenz E, Melzig M, Bienert M. Cellular uptake of an alpha-helical amphipathic model peptide with the potential to deliver polar compounds into the cell interior non-endocytically. *Biochim. Biophys. Acta* 1998; **1414**: 127–139.
17. Frankel AD, Pabo CO. Cellular uptake of the tat protein from human immunodeficiency virus. *Cell* 1988; **55**: 1189–1193.
18. Green M, Loewenstein PM. Autonomous functional domains of chemically synthesized human immunodeficiency virus tat trans-activator protein. *Cell* 1988; **55**: 1179–1188.
19. Vives E, Brodin P, Lebleu B. A truncated HIV-1 Tat protein basic domain rapidly translocates through the plasma membrane and accumulates in the cell nucleus. *J. Biol. Chem.* 1997; **272**: 16010–16017.
20. Perez F, Joliot A, Bloch-Gallego E, Zahraoui A, Triller A, Prochiantz A. Antennapedia homeobox as a signal for the cellular internalization and nuclear addressing of a small exogenous peptide. *J. Cell Sci.* 1992; **102**: 717–722.

21. Joliot A, Le Roux I, Volovitch M, Bloch-Gallego E, Prochiantz A. Neurotrophic activity of a homeobox peptide. *Prog. Neurobiol.* 1994; **42**: 309–311.
22. Derossi D, Joliot AH, Chassaing G, Prochiantz A. The third helix of the Antennapedia homeodomain translocates through biological membranes. *J. Biol. Chem.* 1994; **269**: 10444–10450.
23. Suzuki T, Futaki S, Niwa M, Tanaka S, Ueda K, Sugiura Y. Possible existence of common internalization mechanisms among arginine-rich peptides. *J. Biol. Chem.* 2002; **277**: 2437–2443.
24. Futaki S, Goto S, Sugiura Y. Membrane permeability commonly shared among arginine-rich peptides. *J. Mol. Recognit.* 2003; **16**: 260–264.
25. Rothbard JB, Kreider E, VanDeusen CL, Wright L, Wylie BL, Wender PA. Arginine-rich molecular transporters for drug delivery: role of backbone spacing in cellular uptake. *J. Med. Chem.* 2002; **45**: 3612–3618.
26. Rothbard JB, Jessop TC, Wender PA. Adaptive translocation: the role of hydrogen bonding and membrane potential in the uptake of guanidinium-rich transporters into cells. *Adv. Drug Delivery Rev.* 2005; **57**: 495–504.
27. Ferrari A, Pellegrini V, Arcangeli C, Fittipaldi A, Giacca M, Beltram F. Caveolae-mediated internalization of extracellular HIV-1 tat fusion proteins visualized in real time. *Mol. Ther.* 2003; **8**: 284–294.
28. Wadia JS, Stan RV, Dowdy SF. Transducible TAT-HA fusogenic peptide enhances escape of TAT-fusion proteins after lipid raft macropinocytosis. *Nat. Med.* 2004; **10**: 310–315.
29. Richard JP, Melikov K, Brooks H, Prevot P, Lebleu B, Chernomordik LV. Cellular uptake of unconjugated TAT peptide involves clathrin-dependent endocytosis and heparan sulfate receptors. *J. Biol. Chem.* 2005; **280**: 15300–15306.
30. Ziegler A, Nervi P, Durrenberger M, Seelig J. The cationic cell-penetrating peptide CPP(TAT) derived from the HIV-1 protein TAT is rapidly transported into living fibroblasts: optical, biophysical, and metabolic evidence. *Biochemistry* 2005; **44**: 138–148.
31. Fretz MM, Penning NA, Al-Taei S, Futaki S, Takeuchi T, Nakase I, Storm G, Jones AT. Temperature-, concentration- and cholesterol-dependent translocation of L- and D-octa-arginine across the plasma and nuclear membrane of CD34+ leukaemia cells. *Biochem. J.* 2007; **403**: 335–342.
32. Duchardt F, Fotin-Mleczek M, Schwarz H, Fischer R, Brock R. A comprehensive model for the cellular uptake of cationic cell-penetrating peptides. *Traffic* 2007; **8**: 848–866.
33. Silhol M, Tyagi M, Giacca M, Lebleu B, Vives E. Different mechanisms for cellular internalization of the HIV-1 Tat-derived cell penetrating peptide and recombinant proteins fused to Tat. *Eur. J. Biochem.* 2002; **269**: 494–501.
34. Maiolo JR, Ferrer M, Ottinger EA. Effects of cargo molecules on the cellular uptake of arginine-rich cell-penetrating peptides. *Biochim. Biophys. Acta* 2005; **1712**: 161–172.
35. Alvarez J, Hamplova J, Hohaus A, Morano I, Haase H, Vassort G. Calcium current in rat cardiomyocytes is modulated by the carboxyl-terminal ahnak domain. *J. Biol. Chem.* 2004; **279**: 12456–12461.
36. Hallbrink M, Oehlke J, Papsdorf G, Bienert M. Uptake of cell-penetrating peptides is dependent on peptide-to-cell ratio rather than on peptide concentration. *Biochim. Biophys. Acta* 2004; **1667**: 222–228.
37. Martin RM, Leonhardt H, Cardoso MC. DNA labeling in living cells. *Cytometry A* 2005; **67**: 45–52.
38. Futaki S, Suzuki T, Ohashi W, Yagami T, Tanaka S, Ueda K, Sugiura Y. Arginine-rich peptides. An abundant source of membrane-permeable peptides having potential as carriers for intracellular protein delivery. *J. Biol. Chem.* 2001; **276**: 5836–5840.
39. Goun EA, Pillow TH, Jones LR, Rothbard JB, Wender PA. Molecular transporters: synthesis of oligoguanidinium transporters and their application to drug delivery and real-time imaging. *Chembiochem* 2006; **7**: 1497–1515.
40. Martin RM, Tünnemann G, Leonhardt H, Cardoso MC. Nucleolar marker for living cells. *Histochem. Cell Biol.* 2007; **127**: 243–251.
41. Trehin R, Nielsen HM, Jahnke HG, Krauss U, Beck-Sickinger AG, Merkle HP. Metabolic cleavage of cell-penetrating peptides in contact with epithelial models: human calcitonin (hCT)-derived peptides, Tat(47–57) and penetratin(43–58). *Biochem. J.* 2004; **382**: 945–956.
42. Mosmann T. Rapid colorimetric assay for cellular growth and survival: application to proliferation and cytotoxicity assays. *J. Immunol. Methods* 1983; **65**: 55–63.

DOI: 10.1002/psc

Supplementary figure 1

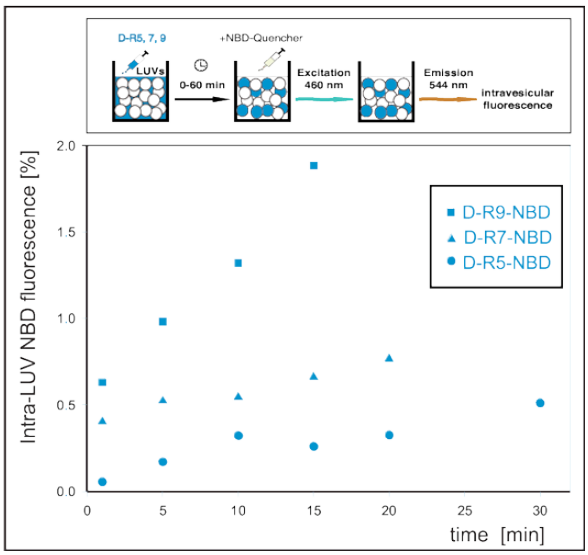

Supplementary Figure 1 Penetration of artificial membranes by oligo-arginines.
LUVs (Large Unilamellar Vesicles) were prepared from a mixture from 70 mol% of DOPC (dioleoylphosphatidylcholine) and 30 mol% of DOPS (dioleoylphosphatidylserine). In total 1 µmol of lipids were mixed in chloroform. A dry lipid film was formed by solvent evaporation under a nitrogen stream. The dried lipids were resolubilized in 2 ml of PBS (pH 7.4) by 5 min of vortexing. To yield LUVs the lipid suspension was processed by freeze/thaw-cycles (5x) and extrusion through a 0.1 µm filter (10x). Consecutive arginines (R5, R7, R9) as D-isomers were synthesized and coupled directly to the NBD (7-nitro-2-1,3-benzoxadiazol-4-yl)-group at the N-terminus by Peptide Specialty Laboratories GmbH (Heidelberg, Germany). For the quenching assay 740 µl of PBS were mixed with 60 µl of LUV suspension and incubated with the NBD-labeled peptides at 5 µM for different time spans. NBD fluorescence from peptides remaining in the exterior of the LUVs was then quenched by adding 25 mM of the non membrane permeable sodium dithionite. Fluorescence was detected with a FluoroMax-4-spectrofluorometer (Horiba Jobin Yvon, Edison, USA). NBD was excited at 460 nm and the fluorescence was recorded at 544 nm. For measuring the maximal quenchable fluorescence of the peptides present in the exterior and also in the interior of the LUVs, 0.5 % Triton X-100 was added afterwards to dissolve the vesicles. Counts for total fluorescence and fluorescence after quenching were corrected by subtracting this non-quenchable fraction. The intravesicular peptide in LUVs was displayed as percentage of total fluorescence after dithionate quenching for the different NBD-peptides (●) R5-NBD, (▲) R7-NBD and (■) R9-NBD. At a first glance the percentage of transduction as measured by the non-quenched intra-LUV peptide fluorescence seemed to be low in comparison to the experiments in living cells. However, under our experimental conditions the total volume of LUVs corresponded to about 0.2 % of the suspension volume assuming a LUV diameter of 100 nm and a surface area of lipids of 0.6 nm2. In the light of this estimate the results indicate an enrichment of peptides in the lumen of LUVs at least for R9.